Measurements of Particles Rebound Characteristics on Materials Used in Gas Turbines

W. Tabakoff*
University of Cincinnati, Cincinnati, Ohio 45221

This paper describes an experimental method used to find the rebound characteristics of small solid particles impacting different materials. Such data are used for particle trajectories and erosion calculations in turbomachinery. The materials which are investigated are: 410 Stainless Steel, 2024 Aluminum, 6A1-4V Titanium, INCO 718, RENE 41, AM355, L605 Cobalt, and Alumina (Al_2O_3). Particle materials are fly ash of 15 μ. In addition, erosion rate equation was developed for INCO 718 that predicts the erosion rates at high temperatures very well.

Nomenclature

A, B, a, n, m = empirical constants
e_β = β_2/β_1 directional coefficient
e_N = V_{N2}/V_{N1} normal restitution ratio
e_T = V_{T2}/V_{T1} tangential restitution ratio
e_v = V_2/V_1 total velocity restitution ratio
V_1 = particle impingement velocity, ft/s
V_2 = particle rebound velocity, ft/s
Y_s = material yield strength at the operating temperature, Kpsi
Y_{SRT} = material yield strength at the ambient temperature, Kpsi
β_1 = particle impingement angle, radians
β_2 = particle rebounding angle, radians
ε = erosion rate, cm^3/gm

Introduction

AIRCRAFT engines operating in areas where the atmosphere is polluted by small solid particles and industrial gas turbines burning coal are examples of machines operating under particulate two-phase flow conditions. The presence of solid particles in the working media leads to a performance deterioration of these engines both structurally and aerodynamically.

Under two-phase flow conditions, the gas and particles experience different degrees of turning as they flow through the blade channels. This is mainly due to the differences in their inertia. The major interacting force between the gas and particles is the viscous drag. The degree of turning and acceleration or deceleration achieved by the particles depends on the ratio of the viscous forces to the inertial forces experienced by the particles. This results in a concentration gradient across the blade channel and causes a change in the properties of gas and particles. The net result is a change in the blade surface pressure distribution, which alters the engine performance during the period of particle ingestion.

If the particles are of erosive nature, the problem becomes more complicated. The impact of particles on the blade surfaces can cause severe erosion damage, that leads to structural failure of the blades. This damage is manifested by pitting and cutting of the blade leading and trailing edges, and a general increase in the blade surface roughness. The overall effect of the above phenomena, from the aerodynamic viewpoint, is an increase in total pressure loss across the blade row.

The use of pulverized coal as fuel in many power plants and industrial establishments is inevitable both now and in the foreseeable future. The major problem confronting earlier developers of coal-burning turbines is the serious erosion of turbine blades and other metal parts by the suspension of fly ash in hot combustion gases. It is possible to remove approximately 85 percent by weight of the ash in these gases using cyclones. However, small particles ranging in size between 1 and 15 μ still pass through the cyclones and enter the turbine. Typical ash concentrations for such a turbine are about 0.000275 mg/cm^3 (7.8 mgm/ft^3). The damage is caused principally by erosion of the leading and trailing edges of the stator and rotor blades. A thorough knowledge of the various parameters that influence the extent of erosion damage is required to improve the life and the aerodynamic performance of turbomachinery operating in an ambient of particulate flow. This paper presents an experimental method used to determine the particle restitution coefficients that are used for trajectory calculations in turbomachinery and in the new derived equations to calculate the material erosion.

Experimental Set-Up

The experimental set-up is shown schematically in Fig. 1. It consists of an erosion wind tunnel and a solid particles feeder.

Erosion Wind Tunnel

An existing erosion wind tunnel was used in this investigation. The major advantages of this tunnel are: controlling the primary variables of fluid velocity, particle velocity, particle flow rate, and particle sizes in a representative aerodynamic environment. Provisions are made in the tester design to allow variation of the angle of attack between the abrasive particle and the surface of the test specimen.

Figure 1 is a schematic description of the apparatus to fulfill these objectives. The equipment functions as follows. A measured amount of dry fly ash is placed into the particle feeder A. The particles are fed into secondary air source and carried up to the particle injector C, where it mixes with the main air supply B. The particles are then accelerated by the high velocity air in a constant area duct D, and impact the specimen in test section E. The test dust is then separated from the air by a cyclone separator G, and collected in the container H. The test air is further filtered through a commercial 5 μ filter F.

The test section is designed such that the particle laden air is channeled over the specimen and the aerodynamics of the

Presented as Paper 89-1693 at the AIAA 24th Thermophysics Conference, Buffalo, NY, June 12–24, 1989; received July 24, 1989; revision received August 10, 1990; accepted for publication Nov. 25, 1990.

*Professor, Department of Aerospace Engineering and Engineering Mechanics. Member AIAA.

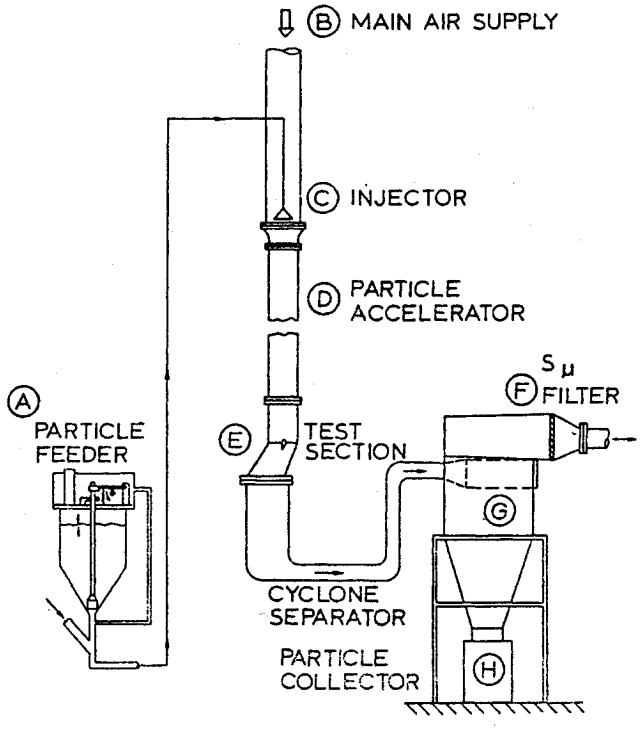

Fig. 1 Schematic of erosion research facility.

fluid surrounding the blade sample are preserved. This section contains several interchangeable inserts so that the fluid profile can be determined using conventional instrumentation, and the particle trajectories can be recorded using high speed photographic or laser methods.

Particle Feeder

The particles from the feeder A (Fig. 1) are carried up to the particle injector. The feeder is designed as a vessel to operate at high air pressures. However, this pressure is equalized above and below the plunger by a bypass line. This allows the system to be calibrated under gravity feed conditions. Further, an electric eye records the plunger rpm so that the operating conditions are maintained. The metering orifice is designed to be replaceable. In this manner, a larger (or smaller) orifice may be used, along with the corresponding rod diameter, to allow versatility of the feeder. In this investigation the air flow was seeded with fly ash. The chemical composition of the fly ash is given in Kotwal and Tabakoff.[1] [Si = 50%; Al = 22%; Fe = 20%; S = 1.2%; the remaining are Mg, Na, Ca, C, and others.]

Laser and Optics (LDV System)

The optical elements of the two-component laser-Doppler anemometer were arranged in the backward scatter mode, to measure two simultaneous velocity components of a single particle using two counter processors. A two-color, 5-W argon-ion Spectra physics, model 164-09, is used as a laser source. The laser beams are brought into one common measuring volume using a transmitting lens of 250-mm focal length. The crossing angle for the incident 1.5-mm diameter beams was 11.05 deg.

Data Acquisition System

Two signal processors TSI model 1990 and on-line Minc 11/23 are used to acquire synchronized data for the simultaneous measurements of two velocity components. The minimum time for a particle to cross the measuring volume was evaluated to be 1.4 μsec. Accordingly, the synchronization condition was set to 1 μsec, which is the time out between the two data ready pulses received from both signal processors. A time out of 5 μsec, after each valid synchronized data point is tagged in the computer; allows the particle to clear the measuring volume. The data acquisition program insures that the sampling data is not obtained more than once from the same particle.

Development of Particle Rebound Correlations

The erosion of metals impacted by small dust particles as well as the rebound dynamics of these particles can only be described in a statistic sense. This becomes obvious when one examines the number of geometric situations that might occur at impact. After an incubation period, the target material will become pitted with craters and in fact after a slightly longer period, a regular ripple pattern may form on the eroded surface. Thus, the local impact angle between the small particle and the eroded surface may deviate considerably from the geometric average. Further, the particles themselves are irregular, crystalline in shape, with several sharp corners. As

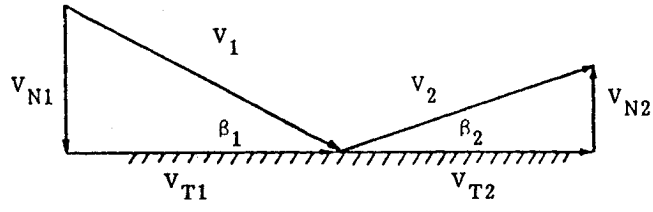

Fig. 2 Velocity and angle notations.

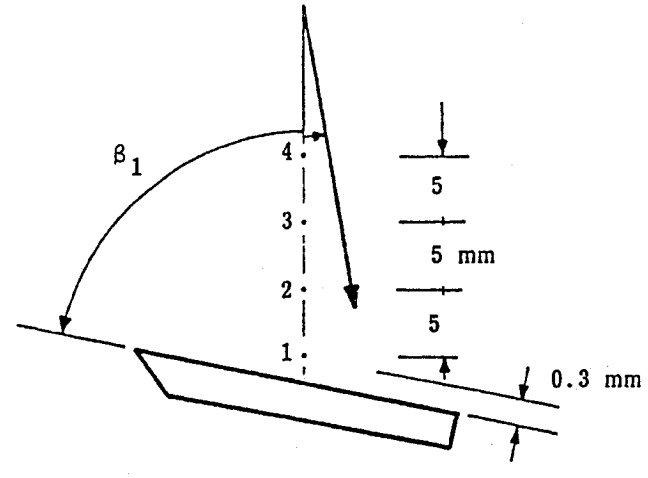

Fig. 3 Impingement measurements locations.

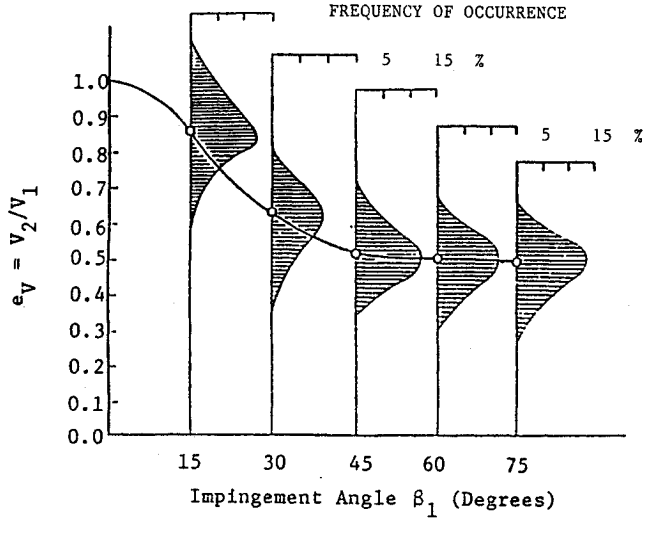

Fig. 4 Influence of impact angle on particle velocity restitution coefficient.

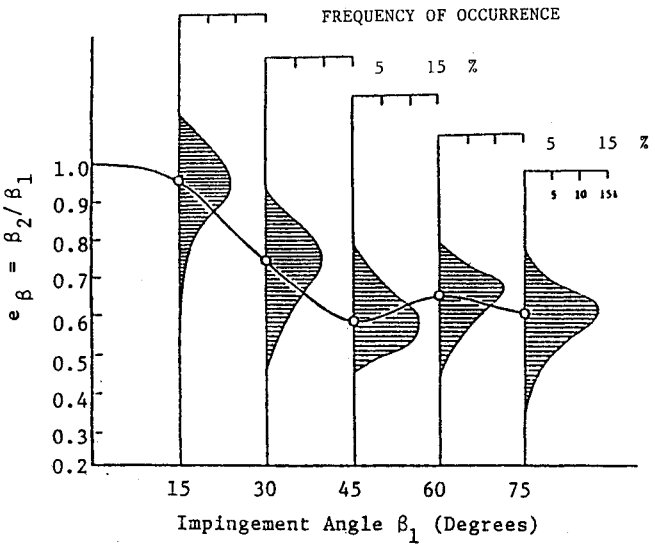

Fig. 5 Influence of impact angle on the particle directional coefficient.

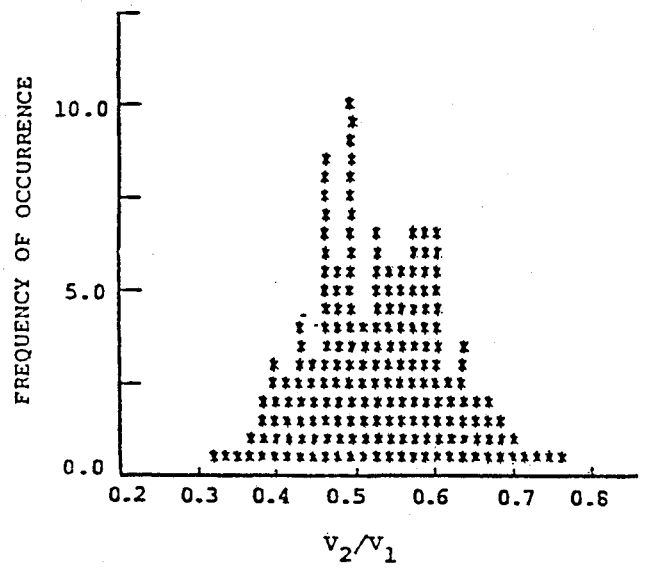

Fig. 6 Erosive particle velocity restitution ratio distribution.

the particle approaches the specimen, the orientation of the particle is, for the most part, random. Some particles will impact on a flat surface and do very little work on the target material. Others will impact with a corner oriented in a manner where it will remove material in a method similar to that of a cutting tool.

The restitution coefficient or restitution ratio is a measure of the kinetic energy exchange between two objects upon impact. Since erosion is a function of the energy exchange between the erodent particle and the material impacted, the restitution ratio will give a good indication of the behavior of the particle-material interaction. In this investigation an erosive impact occurs when the contaminant particle is much harder than the target material.

Grant and Tabakoff[2] were the first to investigate thoroughly the rebound characteristics of high speed eroding particles. The study was carried out on annealed 2024 aluminum alloy. The data was described using histograms to illustrate its statistical distribution. It was concluded that the restitution ratio V_2/V_1, which is directly related to the kinetic energy lost during impact, does not give sufficient information in regard to erosion. With this in mind, the restitution ratio was broken down into a normal velocity restitution ratio V_{N2}/V_{N1}, as shown in Fig. 2 (the normal component of the particle velocity after impact/the normal component of the particle velocity before impact), and a tangential velocity restitution ratio V_{T2}/V_{T1} (the tangential component of the particle velocity after impact/the tangential component of the particle velocity before impact). It was found that the normal velocity restitution ratio does not significantly contribute to ductile erosion. Most probably the kinetic energy is dissipated by plastic deformation of the target material without significant material removal.

Measurement Technique

The LDV system was used to measure the impact and rebound velocities and angles on different material samples for different incidence angles. The impinging particle velocities were measured at four points above the stainless steel sample as shown in Fig. 3.

At point 1 location, the results obtained include the velocities of the smaller fly ash particles, less than 2 μ, which follows the air flow streamlines without hitting the specimen surface. Therefore, the velocity at point 2 was selected to represent the impingement velocity for all impacting angles. Measurements for seven incidence angles β_1 were performed. The velocities are normalized with respect to the particle velocity at the center of the test section that was 98 m/s (320 ft/sec).

The rebounding velocities were measured at four points located on a line 0.3 mm above and parallel to a specimen surface. The ratio of the particle velocity after and before impact, V_2/V_1, is plotted against the angle of attack (β_1) as shown in Fig. 4. Since the statistical distributions are of importance, the shape of these distributions are cross plotted on the figure. The parameter V_2/V_1 is directly related to the kinetic energy lost during impact. The spread in this data indicates the variable condition of the surfaces and the orientation of the particle at impact. It is evident from this figure that V_2/V_1 decreases as the impact angle β_1 increases from zero to 75 deg.

The directional coefficient (β_2/β_1) is plotted in Fig. 5 versus the impact angle β_1. Again, these data are plotted with their statistical distributions.

Figure 6 illustrates a typical histogram of the restitution ratios for the fly ash impacting at $\beta_1 = 60$ deg over a stainless steel sample. The vertical axis at this figure represents the number of times the restitution ratio was found to be between the limits designated by the scale at the horizontal axis. The wide distribution of the data is due to the variations of the particle sizes and shapes irregularity.

Rebounding Results

All the previous results reported in Refs. 3–7 were obtained for an impact angle range of 15 to 75 deg with flat targets and

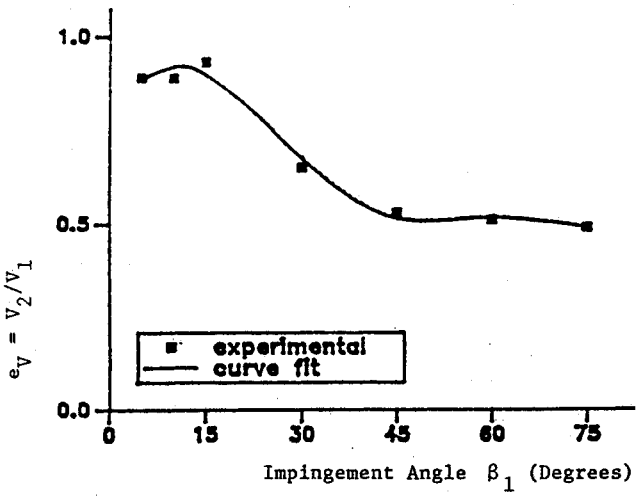

Fig. 7 Influence of impact angle on the erosive particle velocity restitution ratio for 410 stainless steel.

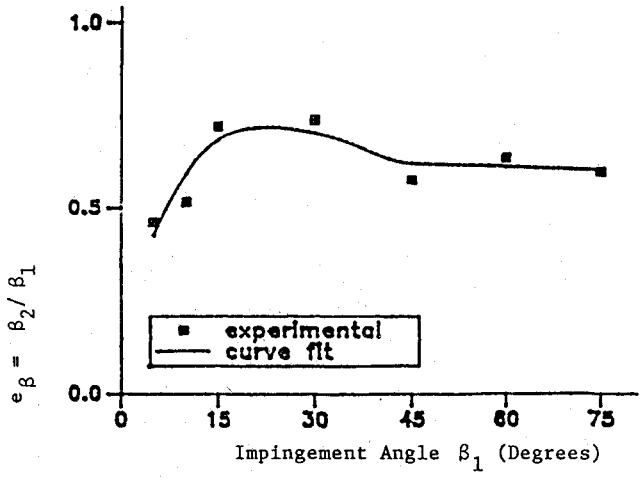

Fig. 8 Influence of impact angle on the erosive particle directional coefficient for 410 stainless steel.

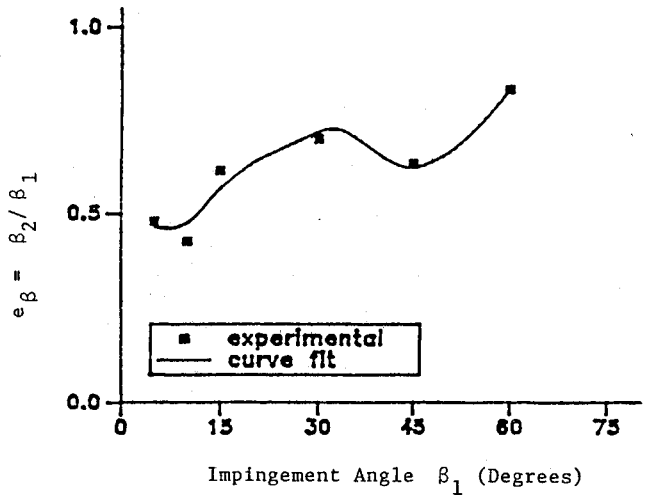

Fig. 10 Influence of impact angle on the erosive particle directional coefficient for 2024 aluminum.

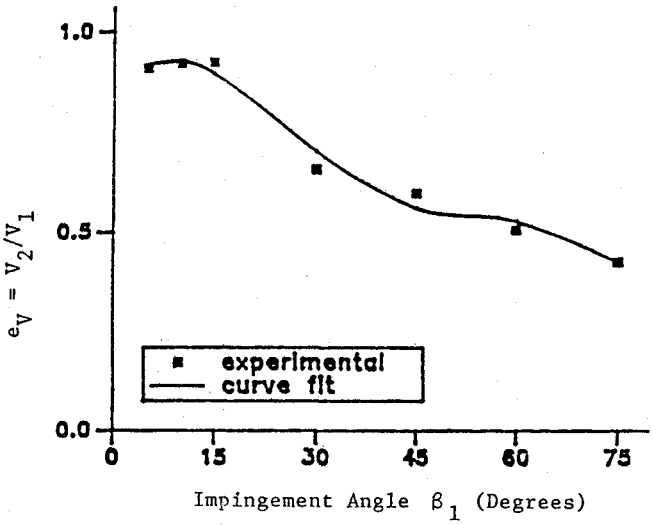

Fig. 9 Influence of impact angle on the erosive particle total velocity restitution ratio for 2024 aluminum.

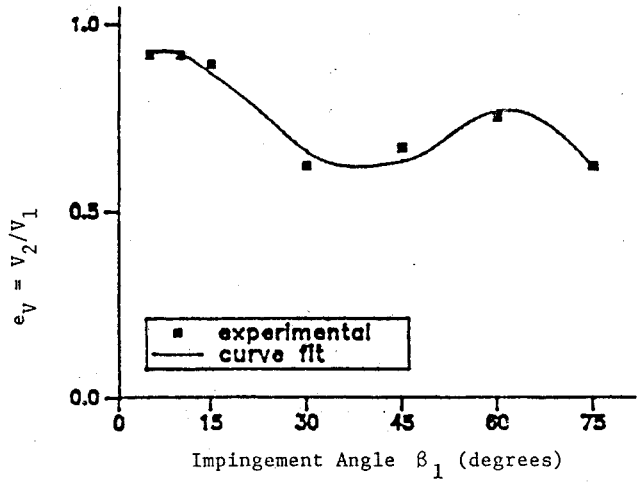

Fig. 11 Influence of impact angle on the erosive particle total velocity restitution ratio for 6 Al-4V titanium.

used the two-component Laser Doppler Velocimeter (LDV) system. The two-dimensional (2-D) particle velocity measurements were conducted in the plane of the impinging particle velocity and normal to the target surface.

This paper presents the restitution ratios starting at small impact angles (less than 15 deg) for eight different materials. Based on the similarity of the rebound characteristics for the tested materials, the particle impact and rebound experiment results are investigated to determine restitution ratio correlations representative of the whole group of blade materials. In all the new tests, 15 μ mean diameter fly ash particles were used. The composition and size range of fly ash particles and the properties for some of the target materials are given in Ref. 3.

The particle trajectory calculations in the gas turbine combustion chambers[8] showed that the particle impact angle with the chamber walls can be very small for fly ash particles. However, experimental data for the restitution ratios were previously obtained for the impact angle, β_1, range of 15 to 75 deg. The information about the restitution ratios out of this range were obtained by extrapolation. In order to increase the accuracy of the restitution ratios at small impact angle range, LDV measurements of impact and rebound velocities were performed for 5 and 10 deg impact angles. The restitution ratios at these small angles were determined for 410 stainless steel, 2024 aluminum, 6A1–4V titanium, INCO 718, RENE 41, AM 355, L605 cobalt, and alumina (Al_2O_3). Combining these new data with the previous restitution ratios, least squares polynomial curve fits of the mean values of the restitution parameters were obtained. These curve fits are shown as solid lines in Figs. 7–20 together with the experimental points.

The total velocity restitution ratio, V_2/V_1, is plotted against the impact angle β_1 in Figs. 7, 9, 11, 13, 15, 17, 19, and 21 for the above specified materials, covering an impact angle range of 5–75 deg.

The directional coefficient, β_2/β_1, is plotted against impact angle β_1 in Figs. 8, 10, 12, 14, 16, 18, 20, and 22 for all the tested materials. The normal, V_{N2}/V_{N1}, and the tangential, V_{T2}/V_{T1}, restitution ratios are also measured and plotted against the impact angle, but the plots are not presented in this paper.

The following empirical equations represent the variation of the various restitution parameters with the impingement angle β_1 according to the curve fits of Figs. 7–22.

410 Stainless Steel:

$$e_V = V_2/V_1 = 0.76 + 2.01\beta_1 - 7.66\beta_1^2 + 8.11\beta_1^3 - 2.72\beta_1^4 \quad \text{(1a)}$$

$$e_\beta = \beta_2/\beta_1 = 0.15 + 3.85\beta_1 - 8.64\beta_1^2 + 7.49\beta_1^3 - 2.25\beta_1^4 \quad \text{(1b)}$$

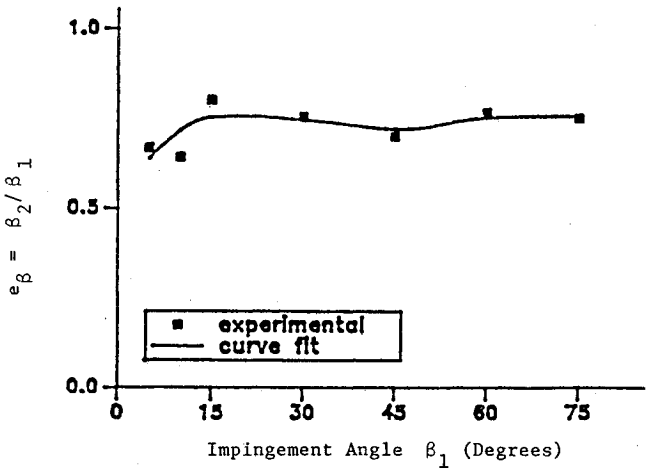

Fig. 12 Influence of impact angle on the erosive particle directional coefficient for 6Al-4V titanium.

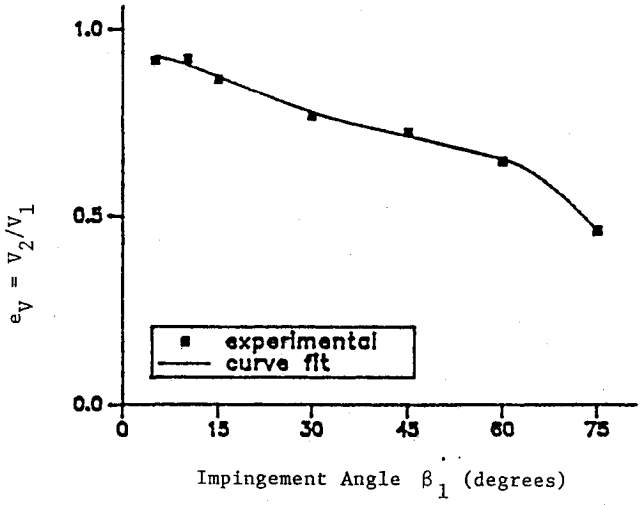

Fig. 13 Influence of impact angle on the erosive particle total velocity restitution ratio for INCO 718.

2024 Aluminum:

$$e_V = V_2/V_1 = 0.85 + 1.20\beta_1 - 5.34\beta_1^2 + 5.86\beta_1^3 - 2.04\beta_1^4 \quad (2a)$$

$$e_\beta = \beta_2/\beta_1 = 0.67 - 4.34\beta_1 + 27.10\beta_1^2 - 58.41\beta_1^3 + 52.14\beta_1^4 - 16.39\beta_1^5, \quad (2b)$$

6A1–4V Titanium:

$$e_V = V_2/V_1 = 0.85 + 1.39\beta_1 - 7.40\beta_1^2 + 9.68\beta_1^3 - 3.78\beta_1^4 \quad (3a)$$

$$e_\beta = \beta_2/\beta_1 = 0.51 + 1.89\beta_1 - 4.74\beta_1^2 + 4.57\beta_1^3 - 1.48\beta_1^4 \quad (3b)$$

INCO 718:

$$e_V = V_2/V_1 = 0.94 - 1.39\beta_1^2 + 1.99\beta_1^3 - 0.87\beta_1^4 \quad (4a)$$

$$e_\beta = \beta_2/\beta_1 = 0.52 + 0.34\beta_1 + 0.78\beta_1^2 - 2.49\beta_1^3 + 1.26\beta_1^4 \quad (4b)$$

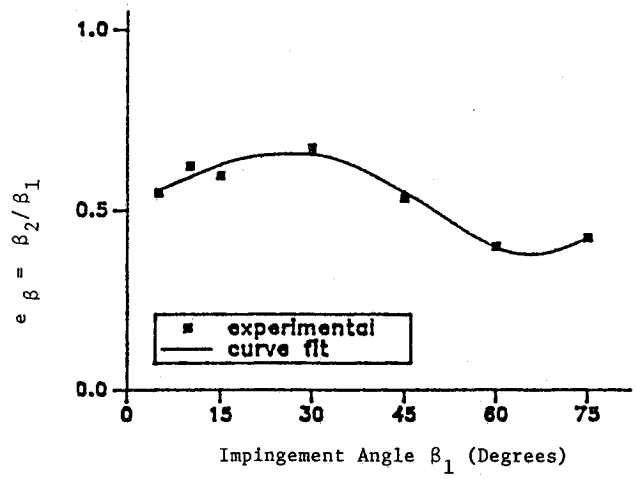

Fig. 14 Influence of impact angle on the erosive particle directional coefficient for INCO 718.

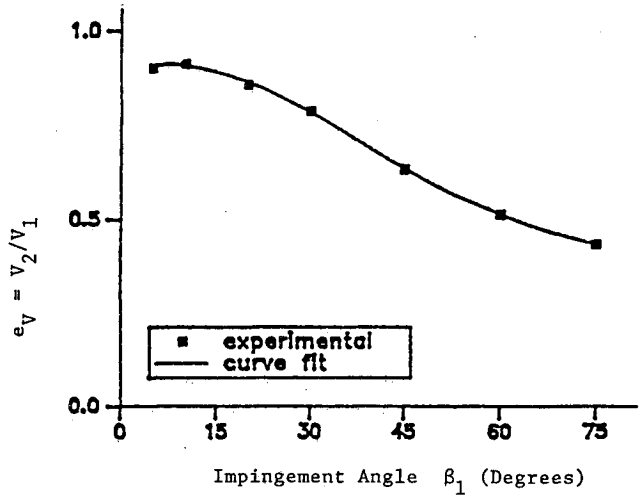

Fig. 15 Influence of impact angle on the erosive particle total velocity restitution ratio for RENE 41.

RENE 41:

$$e_V = V_2/V_1 = 0.88 + 0.44\beta_1 - 1.80\beta_1^2 + 1.32\beta_1^3 - 0.30\beta_1^4 \quad (5a)$$

$$e_\beta = \beta_2/\beta_1 = 0.40 + 2.11\beta_1 - 4.37\beta_1^2 + 3.67\beta_1^3 - 1.14\beta_1^4 \quad (5b)$$

AM 355 Steel Alloy:

$$e_V = V_2/V_1 = 0.89 + 0.47\beta_1 - 2.86\beta_1^2 + 3.05\beta_1^3 - 1.04\beta_1^4 \quad (6a)$$

$$e_\beta = \beta_2/\beta_1 = 0.29 + 2.23\beta_1 - 7.52\beta_1^2 + 9.61\beta_1^3 - 3.85\beta_1^4 \quad (6b)$$

L605 Cobalt:

$$e_V = V_2/V_1 = 0.82 + 1.48\beta_1 - 6.63\beta_1^2 + 7.78\beta_1^3 - 2.88\beta_1^4 \quad (7a)$$

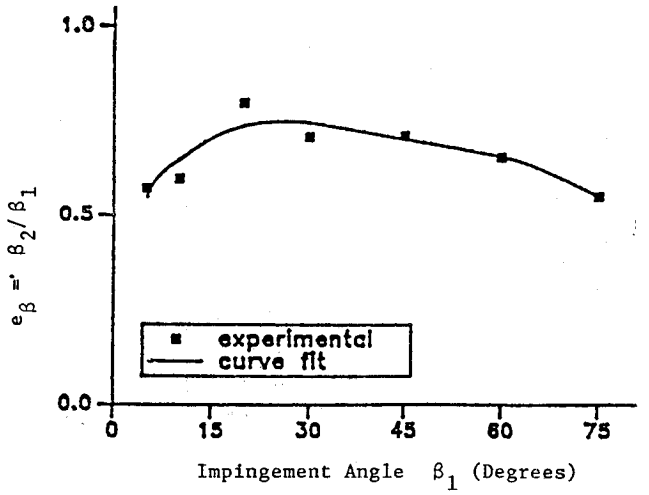

Fig. 16 Influence of impact angle on the erosive particle directional coefficient for RENE.

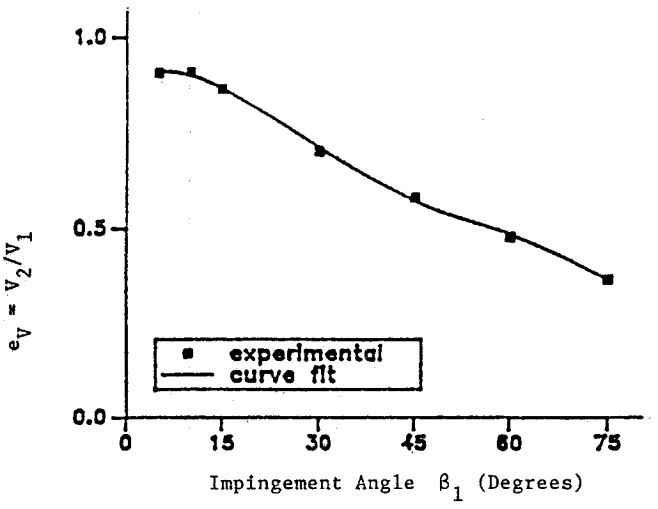

Fig. 17 Influence of impact angle on the erosive particle total velocity restitution ratio for AM 355.

$$e_\beta = \beta_2/\beta_1 = 0.6 - 4.59\beta_1 + 32.65\beta_1^2 - 74.09\beta_1^3 + 67.28\beta_1^4 - 21.11\beta_1^5 \quad (7b)$$

Alumina (Al_2O_3):

$$e_V = V_2/V_1 = 0.83 + 1.28\beta_1 - 4.85\beta_1^2 + 4.75\beta_1^3 - 1.52\beta_1^4 \quad (8a)$$

$$e_\beta = \beta_2/\beta_1 = 0.93 - 8.39\beta_1 + 46.70\beta_1^2 - 96.46\beta_1^3 + 83.25\beta_1^4 - 25.28\beta_1^5 \quad (8b)$$

where β_1 is measured in radians and these equations are valid within the impact angle range 5–75 deg.

Generalized Restitution Correlations for Fly Ash

Since the same 15 μ mean diameter fly ash particles and the same test conditions were used in all the experiments, the difference in the results are due to the target material effect. Although the differences in the restitution ratios are quite large at some of the impact angles, the general particle rebound characteristics are similar most of the time. This suggests possible generalized correlations for all the target materials. Based on this, the particle impact and rebound experiment results for the tested materials were investigated to determine restitution ratio correlations representative of the whole group of blade materials.

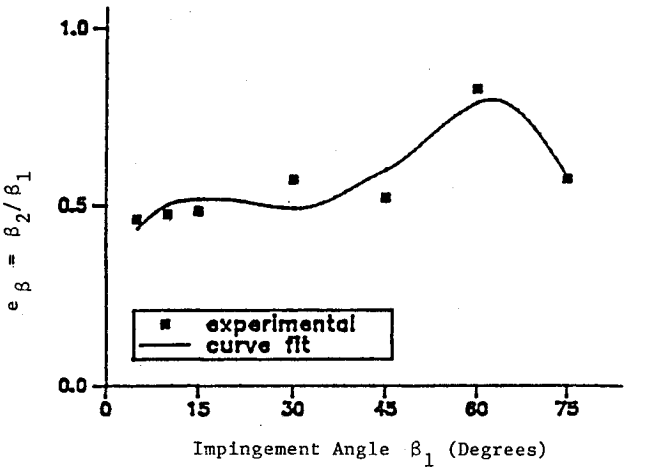

Fig. 18 Influence of impact angle on the erosive particle directional coefficient for AM 355.

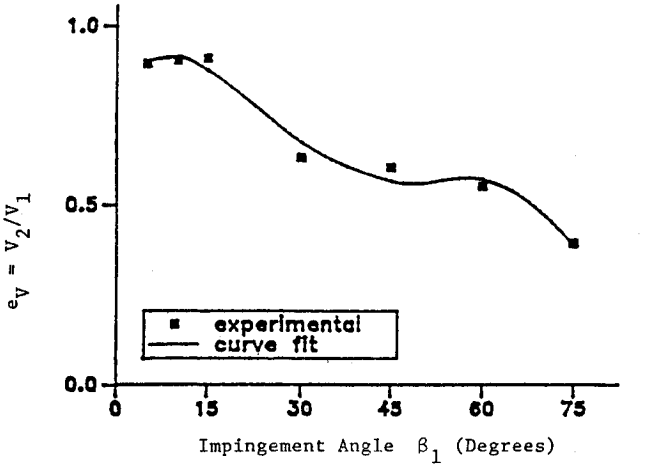

Fig. 19 Influence of impact angle on the erosive particle total velocity restitution ratio for L605 cobalt.

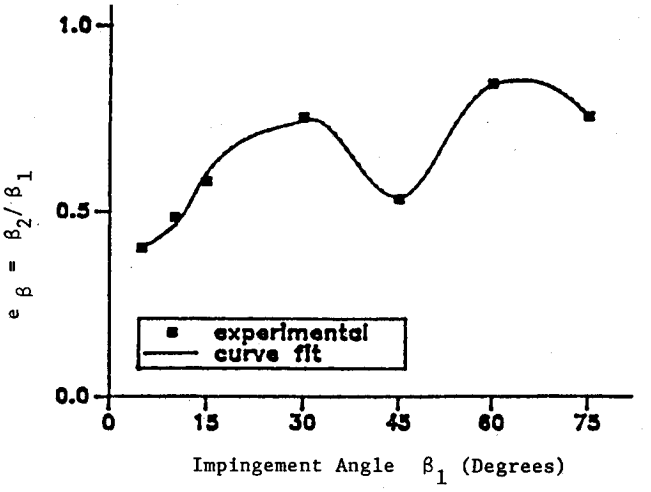

Fig. 20 Influence of impact angle on the erosive particle directional coefficient for L605 cobalt.

First, the averages of the mean restitution ratios for the tested materials were calculated at various impact angles. Least squares polynomial curve fits were then obtained for the averages. Figures 23–26 show these curve fits together with the experimental results. The maximum and minimum values for

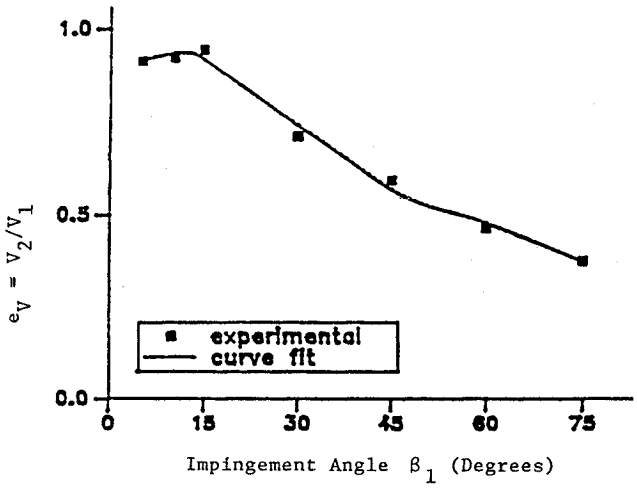

Fig. 21 Influence of impact angle on the erosive particle total velocity restitution ratio for alumina (Al_2O_3)

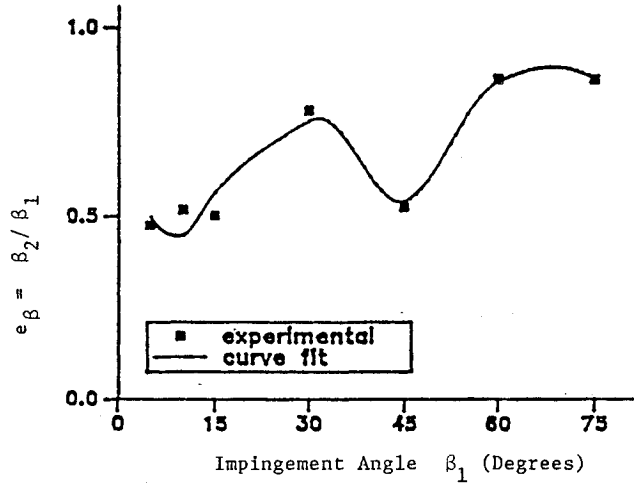

Fig. 22 Influence of impact angle on the erosive particle directional coefficient for alumina (Al_2O_3).

the mean restitution ratios used to determine the limits within the proposed average polynomials are valid. Least squares polynomial curve fits were finally obtained for the limit values. Figures 23–26 show these limit polynomials as dashed lines.

The expressions for the polynomial curve fits the averages of mean restitution ratios are as follows:

$$e_V = V_2/V_1 = 0.85 + 1.07\beta_1 - 4.87\beta_1^2 + 5.46\beta_1^3 - 1.95\beta_1^4 \quad (9a)$$

$$e_\beta = \beta_2/\beta_1 = 0.33 + 2.13\beta_1 - 4.96\beta_1^2 + 4.83\beta_1^3 - 1.65\beta_1^4 \quad (9b)$$

$$e_N = V_{N2}/V_{N1} = 0.30 + 2.17\beta_1 - 6.27\beta_1^2 + 6.46\beta_1^3 - 2.24\beta_1^4 \quad (9c)$$

$$e_T = V_{T2}/V_{T1} = 0.93 - 0.05\beta_1 - 0.28\beta_1^2 - 0.53\beta_1^3 + 0.69\beta_1^4 \quad (9d)$$

The polynomial curve fits specifying the upper limits:

$$e_V = V_2/V_1 = 0.82 + 1.53\beta_1 - 5.92\beta_1^2 + 6.85\beta_1^3 - 2.53\beta_1^4 \quad (10a)$$

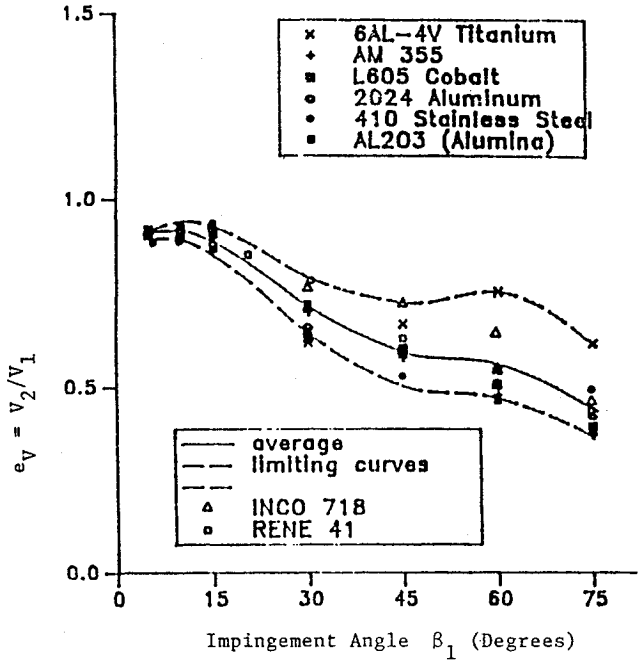

Fig. 23 Average polynomial for the influence of impingement angle on the total velocity restitution ratio.

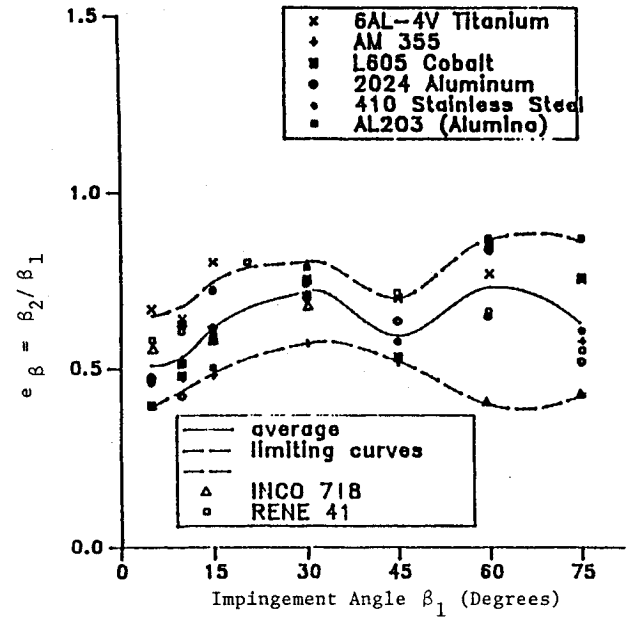

Fig. 24 Average polynomial for the influence of impingement angle on the particle directional coefficient.

$$e_\beta = \beta_2/\beta_1 = 0.48 + 2.11\beta_1 - 5.42\beta_1^2 + 5.50\beta_1^3 - 1.85\beta_1^4 \quad (10b)$$

$$e_N = V_{N2}/V_{N1} = 0.40 + 2.83\beta_1 - 9.03\beta_1^2 + 9.99\beta_1^3 - 3.58\beta_1^4 \quad (10c)$$

$$e_T = V_{T2}/V_{T1} = 0.91 + 0.24\beta_1 - 0.61\beta_1^2 - 0.16\beta_1^3 + 0.62\beta_1^4 \quad (10d)$$

The polynomial curve fits specifying the lower limits:

$$e_V = V_2/V_1 = 0.84 + 1.02\beta_1 - 5.12\beta_1^2 + 5.80\beta_1^3 - 2.06\beta_1^4 \quad (11a)$$

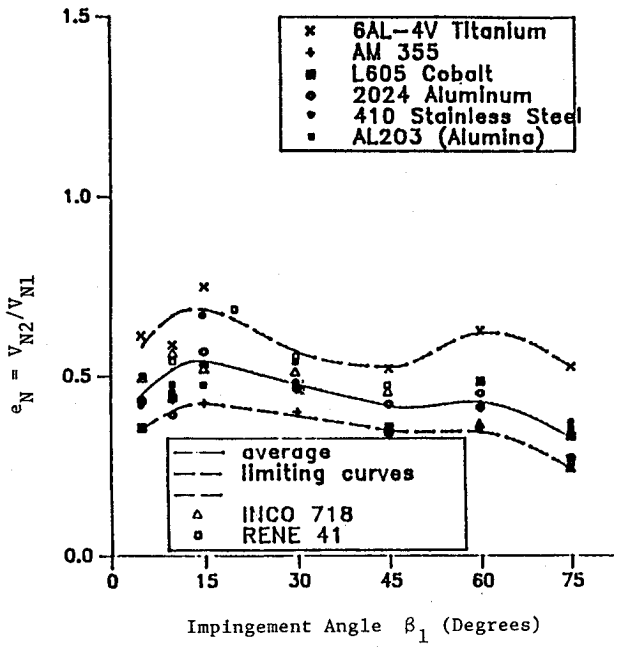

Fig. 25 Average polynomial for the influence of impingement angle on the normal velocity restitution ratio.

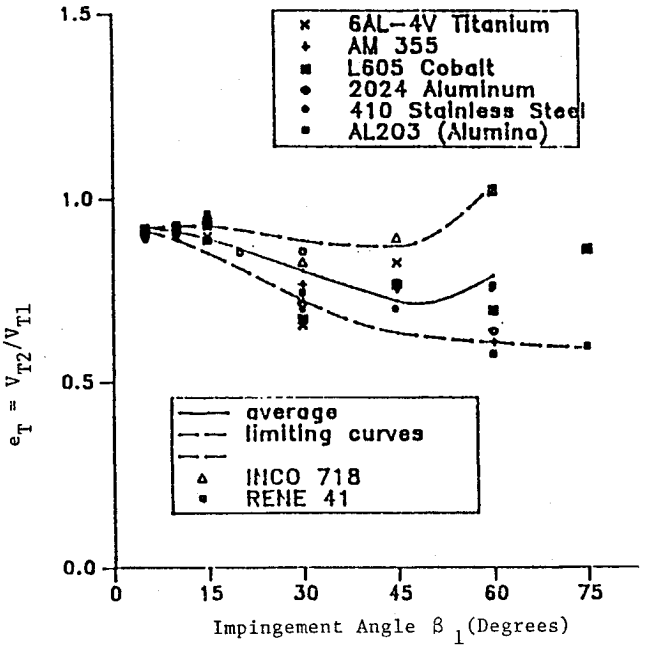

Fig. 26 Average polynomial for the influence of impingement angle on the tangential velocity restitution ratio.

$$e_\beta = \beta_2/\beta_1 = 0.36 + 0.33\beta_1 + 1.33\beta_1^2 - 2.97\beta_1^3 + 1.37\beta_1^4 \quad (11b)$$

$$e_N = V_{N2}/V_{N1} = 0.25 + 1.52\beta_1 - 4.25\beta_1^2 + 4.37\beta_1^3 - 1.53\beta_1^4 \quad (11c)$$

$$e_T = V_{T2}/V_{T1} = 0.92 + 0.07\beta_1 - 1.67\beta_1^2 + 1.96\beta_1^3 - 0.66\beta_1^4 \quad (11d)$$

where β_1 is in radians. These equations are valid within the impact angle range of 5–75 deg.

Erosion Prediction

Semi-empirical erosion rate equations were developed for 2024 aluminum, INCO 718, RENE 41, and AM 355 alloys from the experimental erosion results[3,9,10] for fly ash and silica sand particles of 15 and 165 μ mean diameters, respectively, at various particle velocities and material temperatures. The general form of the semi-empirical erosion rate equation was determined based on the theoretical considerations and knowledge of important parameters such as the work input into the target material due to the particle impacts and the particle restitution ratios.[10,11] In the following equation, the temperature effect on erosion is implicitly introduced through the dependency of material yield strength on temperature.

$$\varepsilon = A\left\{\left(\frac{Y_{SRT}}{Y_S}\right)^a + \left(\frac{Y_S}{Y_{SRT}}\right) - 1\right\}\left[\left(\frac{V_1}{100}\right)^n \cos^n\beta_1 \cdot (1 - e_T^2) + B\left(\frac{V_1}{100}\right)^m \sin^m\beta_1(1 - e_N^2)\right] \quad (12)$$

Note that the variables at the right side of the equation are in English units, whereas the erosion rate term at the left side is expressed in SI units. The conversion between these units is accounted for in the constant A.

The values of the constants of Eq. (12) were determined from a multiple regression analysis of the erosion results reported in Refs. 3, and 9–11. The material properties were obtained from Ref. 12. The following erosion rate equation was developed for INCO 718 alloy using 15 μ mean diameter fly ash particles.

$$\varepsilon = 0.0928 \times 10^{-4}\left[\left(\frac{Y_{SRT}}{Y_S}\right)^{2.9} + \left(\frac{Y_S}{Y_{SRT}}\right) - 1\right] \cdot \left\{\left(\frac{V_1}{100}\right)^{2.0} \cos^{2.0}\beta_1(1 - e_T^2) + 0.171\left(\frac{V_1}{100}\right)^{1.9} \sin^{1.9}\beta_1(1 - e_N^2)\right\} \quad (13)$$

where ε is in cm^3/gm and the restitution coefficients e_T and e_N can be obtained using previous expressions. Comparison with the limited experimental data shows reasonable agreement.

Conclusions

The range of experimental particle rebound data was extended to smaller impact angles (5–15 deg) which are frequently encountered in combustion chambers. New expressions were derived for the restitution characteristics combining the new experimental data for the smaller impact angles with the previous data. These expressions were obtained for 410 stainless steel, 2024 aluminum, 6A1-4V titanium, INCO 718, RENE 41, AM 355, L605 cobalt, and alumina (Al_2O_3), and are valid within the impact angle range of 5–75 deg.

Generalized rebound correlations were generated for the tested target materials and 15 μ mean diameter fly ash particles. These generalized correlations are representative of the whole group of materials within the upper and lower limits which were also specified.

In addition, a semi-empirical erosion rate equation was developed for INCO 718. In general, this equation predicts erosion rates reasonably well. This data will be very useful for particle trajectory calculations in different power systems and for improved erosion calculations at high temperatures.

Acknowledgments

This research work was sponsored by the U.S. Department of Energy Contract No. 19X-89628C, Oak Ridge National

Laboratory, Oak Ridge, Tennessee. We gratefully acknowledge our useful discussions with Rod Judkins, Fossil Energy Material Program Research Office, Oak Ridge.

References

[1]Kotwal, R., and Tabakoff, W., "A New Approach for Erosion Prediction Due to Fly Ash," *Journal of Engineering for Power*, Vol. 103, No. 2, 1981, pp. 265–270.

[2]Grant, G., and Tabakoff, W., "Erosion Prediction in Turbomachinery Resulting from Environmental Solid Particles," *Journal of Aircraft*, Vol. 12, No. 5, 1975, pp. 471–478.

[3]Tabakoff, W., Hamed, A., and Eroglu, H., "Study of Particle Rebound Characteristics and Material Erosion at High Temperature," Fossil Energy Materials Program, U.S. Department of Energy, Tech. Rept., ORNL/Sub/84-89628/01, Dec. 1986.

[4]Tabakoff, W., Hamed, A., and Eroglu, H., "UCIN-3 Study of Particle Rebound Characteristics and Material Erosion at High Temperature," Fossil Energy Materials Program, Quarterly Progress Reports, September 1984, December 1984, March 1985, June 1985, September 1985, December 1985, March 1986 and September 1986.

[5]Tabakoff, W., and Malak, M. F., "Laser Measurements of Fly Ash Rebound Parameters for Use in Trajectory Calculations," *Proceedings of the International Gas Turbine Conference and Exhibit*, ASME Paper 85-GT-161 Houston, TX, March 18–21, 1985.

[6]Tabakoff, W., and Hamed, A., "Laser Measurements of Solid Particles Rebound Parameters Impacting on 2024 Aluminum and 6A1-4V Titanium Alloys," *AIAA Journal of Aeronautics and Astronautics*, Vol. 25, No. 5, 1987, pp. 721–726.

[7]Tabakoff, W., "Study of Particle Rebound Characteristics and Material Erosion at High Temperatures," Fossil Energy Materials Program Conference Proceedings, U.S. Department of Energy, ORNL/FMP-87/4, pp. 492–516.

[8]Tabakoff, W., and Elfeki, S., "Study of Particulate Flow Through a Jet Engine Combustion Chamber," AIAA Eighth International Symposium on Air Breathing Engines, Cincinnati, Ohio, June 1987, pp. 669–680.

[9]Kotwal, R., and Tabakoff, W., "A New Approach for Erosion Prediction Due to Fly Ash," *Journal of Engineering for Power*, Vol. 103, No. 2, 1981, pp. 265–270.

[10]Wakeman, T., and Tabakoff, W., "Measured Particle Rebound Characteristics Useful for Erosion Prediction," ASME Paper 82-GT-170.

[11]Hutchings, I. M., "Some Comments on the Theoretical Treatment of Erosive Particle Impacts," Proceedings, Particle and Droplet Erosion, Cambridge, England, 1979.

[12]*Aerospace Structural Metals Handbook*, Syracuse University Press, 1963.